Effects of mesh irregulaties on accuracy of finite-volume discretization schemes

Boris Diskin* James L. Thomas†

The effects of mesh irregularities on accuracy of unstructured node-centered finite-volume discretizations are considered. The focus is on an edge-based approach that uses unweighted least-squares gradient reconstruction with a quadratic fit. For inviscid fluxes, the discretization is nominally third order accurate on general triangular meshes. For viscous fluxes, the scheme is an average-least-squares formulation that is nominally second-order accurate and contrasted with a common Green-Gauss discretization scheme. Gradient errors, truncation errors, and discretization errors are separately studied according to a previously introduced comprehensive methodology. The methodology considers three classes of grids: isotropic grids in a rectangular geometry, anisotropic grids typical of adapted grids, and anisotropic grids over a curved surface typical of advancing-layer grids. The meshes within the classes range from regular to extremely irregular including meshes with random perturbation of nodes. Recommendations are made concerning the discretization schemes that are expected to be least sensitive to mesh irregularities in applications to turbulent flows in complex geometries.

I. Introduction

Traditional mesh-quality metrics tend to assess meshes without taking into account the type of equations being solved, solutions, or the desired computational output. The most widely-used mesh quality metrics are geometric in nature, considering shape, size, angles, aspect ratio, skewness, Jacobian, etc., of the mesh elements. Additional considerations include variations between mesh elements, such as cell-to-cell and face-to-face ratios, line smoothness, etc. Some schools of thought argue that an accurate and efficient solution can be obtained only on "pretty" meshes similar to either structured Cartesian meshes or to meshes composed from identical perfect elements (perfect triangles, tetrahedrals, etc.) This idea is in direct contradiction with the common Computational Fluid Dynamics (CFD) practice, in which accurate solutions are computed on practical meshes that would be characterized as unacceptable by most geometric mesh quality metrics. Moreover, the most powerful state-of-art method for improving solution accuracy, output-based mesh adaptation,[1] tends to produce "ugly" meshes, but provides vast improvements of the accuracy-per-degree-of-freedom ratio.[2] It is widely recognized today that mesh quality indicators should involve sufficient information about the solution.[3–5] In fact, it is envisioned that the connection should go even deeper and involve modern error-estimation techniques that take into account the specifics of the discretization method in use and the desired computational output.

Historically, mesh quality analyses were first performed for finite-difference and finite-element methods. It is not straightforward to translate those approaches to finite-volume discretizations (FVD) that represent the state of art in CFD computations. While there is no doubt that certain mesh characteristics critically affect accuracy of CFD solutions and gradients, the precise nature of this influence (what affects what) is far from clear.

For finite-difference approaches most of the mesh quality methods try to establish connections between mesh and truncation error.[6,7] The truncation error analysis is often applied to FVD schemes as well.[8] However, it has been long

*National Institute of Aerospace (NIA), 100 Exploration Way, Hampton, VA 23681, USA, Associate Fellow AIAA bdiskin@nianet.org. Also Department of Mechanical and Aerospace Engineering, University of Virginia, Charlottesville, VA 22904, USA. Supported by NASA Fundamental Aeronautics Program, Supersonics Project, NRA Contract NNL07AA23C (PI: Prof. N. K. Yamaleev).

†Computational AeroSciences Branch, NASA Langley Research Center, Mail Stop 128, Fellow AIAA, James.L.Thomas@nasa.gov.

known, that truncation errors of FVD schemes on unstructured grids are not reliable estimators of discretization errors. The *supra-convergence* of discretization errors observed and studied for at least 50 years indicates that design-order accurate FVD solutions can be computed on unstructured grids even when truncation errors exhibit a lower-order convergence or, in some cases, do not converge at all.[9–11]

The theory and applications of mesh quality assessments are well developed and widely used within the finite-element community. While initial groundbreaking work focused on pure geometrical mesh-quality metrics, such as large angles,[12,13] the later developments take solution into account.[14] The standard finite-element estimates use Sobolev norms that simultaneously estimate errors in the solution and its derivatives. These estimates might be too conservative because recent finite-volume computations indicate that accurate solutions can be obtained in spite of formally poor accuracy of gradients.[15–17]

Previously, the effects of mesh irregularities on accuracy of unstructured finite-volume discretizations were evaluated for various common node-centered and cell-centered schemes.[15,16,18–20] The focus here is on an edge-based node-centered approach that uses unweighted least-squares gradient reconstruction with a quadratic fit. For inviscid fluxes, the discretization is nominally third order accurate on general triangular meshes.[21,22] For viscous fluxes, the scheme is an average-least-squares formulation that is contrasted with a common Green-Gauss discretization scheme. These schemes can be formulated as edge-based schemes on general simplicial grids.[23] The inviscid and averaged-least-squares viscous discretizations can be formulated as edge-based on arbitrary grids, including grids used in agglomeration multigrid.[24,25]

Gradient errors, truncation errors, and discretization errors are separately studied according to a previously introduced comprehensive methodology.[15,16] A linear convection equation,

$$(\mathbf{a} \cdot \nabla) U = f, \tag{1}$$

with a velocity vector, $\mathbf{a}$, serves as a model for inviscid fluxes. Poisson's equation

$$\Delta U = f, \tag{2}$$

subject to Dirichlet boundary conditions serves as a model for viscous fluxes. The method of manufactured solutions is used, so the exact solutions and forcing functions, f, are known. Solutions are chosen to be smooth on all grids considered, i.e., no accuracy degradation occurs because of a lack of solution smoothness.

The paper is organized as following. First, grids, FVD schemes, and accuracy measures are briefly described. Then, numerical studies of the FVD accuracy measures are reported for grids of three classes representing isotropic, adapted, and turbulent-flow grids. Conclusions and recommendations are offered at the end.

II. Grids

Computational studies are conducted on two-dimensional grids ranging from structured (regular) grids to irregular grids composed of arbitrary mixtures of triangles and quadrilaterals. Highly irregular (bad quality) grids are deliberately constructed through random perturbations of structured grids. Three classes of grids are considered. Class (A) involves isotropic grids in a rectangular geometry. Class (B) involves highly anisotropic grids, typical of those encountered in grid adaptation. Class (C) involves advancing-layer grids varying strongly anisotropically over a curved body, typical of those encountered in high-Reynolds number turbulent flow simulations.

Four basic grid types are considered: (I) *regular quadrilateral* (i.e., mapped Cartesian) grids; (II) *regular triangular grids* derived from the regular quadrilateral grids by the same diagonal splitting of each quadrilateral; (III) *random triangular grids*, in which regular quadrilaterals are split by randomly chosen diagonals, each diagonal orientation occurring with a probability of half; and (IV) *random mixed-element grids*, in which regular quadrilaterals are randomly split or not split by diagonals; the splitting probability is half; in case of splitting, each diagonal orientation is chosen with probability of half. Nodes of any basic-type grid can be perturbed from their initial positions by random shifts, thus leading to four additional *perturbed* grid types which are designated by the subscript p as (I_p)-(IV_p). The

random node perturbation in each dimension is typically defined as $\frac{1}{4}\rho h$, where $\rho \in [-1, 1]$ is a random number and h is the local mesh size along the given dimension. The representative grids of Class (A) are shown in Figure 1.

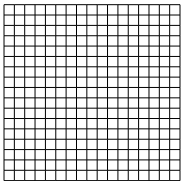

(a) Type (I): regular quadrilateral grid.

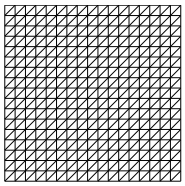

(b) Type (II): regular triangular grid.

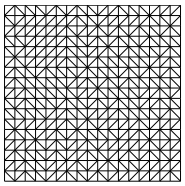

(c) Type (III): random triangular grid.

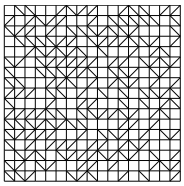

(d) Type (IV): random mixed grid.

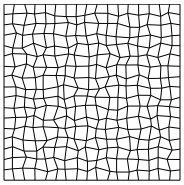

(e) Type (I_p): perturbed quadrilateral grid.

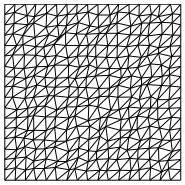

(f) Type (II_p): perturbed triangular grid.

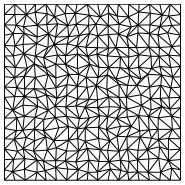

(g) Type (III_p): perturbed random triangular grid.

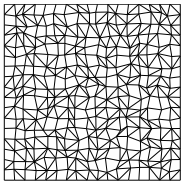

(h) Type (IV_p): perturbed random mixed grid.

Figure 1. Typical regular and irregular grids.

III. Finite-Volume Discretization Schemes

The FVD schemes are derived from the integral form of a conservation law

$$\oint_{\partial\Omega} (\mathbf{F} \cdot \hat{\mathbf{n}})\, ds = \int_{\Omega} f d\Omega, \tag{3}$$

where Ω is a control volume with boundary $\partial\Omega$, $\hat{\mathbf{n}}$ is the outward unit normal vector, and ds is the area differential. The general FVD approach requires partitioning the domain into a set of non-overlapping control volumes and numerically implementing equation (3) over each control volume.

Node-centered discretization schemes are considered, in which solutions are defined at the primal mesh nodes. The control volumes are constructed around the mesh nodes by the median-dual partition: the centers of primal cells are connected with the midpoints of the surrounding faces. These non-overlapping control volumes cover the entire computational domain and compose a mesh that is dual to the primal mesh. The node-centered discretization schemes employ the same degrees of freedom on grids of all types; thus, accuracy is not influenced by a variation in degrees of freedom.

For inviscid Eq. 1, the numerical flux,

$$\left(\mathbf{F}^{\mathbf{h}} \cdot \hat{\mathbf{n}}\right) \equiv U^h \left(\mathbf{a} \cdot \hat{\mathbf{n}}\right), \tag{4}$$

at a control-volume boundary is computed according to the flux-difference-splitting scheme,[26]

$$U^h \left(\mathbf{a} \cdot \hat{\mathbf{n}}\right) = \frac{1}{2} \left(U_L + U_R\right) \left(\mathbf{a} \cdot \hat{\mathbf{n}}\right) - \frac{1}{2} \left|\left(\mathbf{a} \cdot \hat{\mathbf{n}}\right)\right| \left(U_R - U_L\right), \tag{5}$$

where first and second terms represent the flux average and the dissipation, respectively; U_L and U_R are the "left" and "right" solutions linearly reconstructed at the edge midpoint by using solutions and gradients defined at the nodes connected by the edge. The edge-based flux integration scheme approximates the integrated flux through the two faces linked at the edge midpoint by $U^h\left(\mathbf{a}\cdot\mathbf{n}\right)$, where $\mathbf{n}$ is the combined-directed-area vector. The integration scheme is computationally efficient. For exact fluxes, the integration scheme provides third-order accuracy on regular simplicial grids of type (II), second-order accuracy on regular quadrilateral and general simplicial grids of types $(I), (III), (II_p)$, and (III_p), and first-order accuracy on mixed-element and perturbed quadrilateral grids of types $(IV), (IV_p)$, and (I_p).[18,19,27] Second-order unweighted least-squares (ULSQ) gradient reconstruction employing a quadratic fit is used. It was shown that with such gradients, third order discretization accuracy is achieved on simplicial grids.[21,22] The results in the references were obtained with the weighted least-squares gradients, but the third order accuracy has been confirmed by the authors of this paper for ULSQ gradients as well. In (infrequent) cases when the least-squares stencil of the nearest edge-connected neighbors is not sufficient for a quadratic fit, the stencil is expanded to include neighbors of neighbors. Note that five neighbors are typically sufficient for a quadratic fit. On triangular grids considered in this study, the average number of edge-connected neighbors is six; and the minimum number of edge-connected neighbors for an interior node on any grid is four.

For viscous Eq. 2, the numerical flux is defined as

$$\left(\mathbf{F^h}\cdot\hat{\mathbf{n}}\right)\equiv\left(\nabla^{\mathbf{r}}U\cdot\hat{\mathbf{n}}\right), \tag{6}$$

where $\nabla^{\mathbf{r}}U$ is the gradient reconstructed at the face of the control volume. Two gradient reconstruction schemes are considered: (1) The Green-Gauss (GG) scheme[15,28] computes gradients at the primal elements and uses them in face-gradient computations at control-volume boundaries. The GG scheme is widely used in node-centered codes and equivalent to a Galerkin finite-element (linear-element) discretization for triangular/tetrahedral grids. (2) The averaged least-squares (Avg-LSQ) scheme averages the ULSQ gradients at the nodes to compute the face gradient.[24,25] Both schemes use the edge gradient to augment the face gradient and increase the h-ellipticity[29] of the diffusion operator[15,23] and, thus, avoid checkerboard instabilities. The gradient augmentation is introduced in the face-tangent form.[25] Note that when the edge is normal to the face, the edge gradient is the only contributor to the flux. For the GG scheme, the augmentation does not affect the face gradient within a triangular element. It has been shown[18,19,24,25] that the schemes possess second-order accuracy for viscous fluxes on general mixed-element grids.

IV. Accuracy Measures

The accuracy of FVD schemes is analyzed for known exact or manufactured solutions. The forcing function and boundary values are found by substituting this solution into the governing equations, including boundary conditions. The discrete forcing function is defined at the nodes. Boundary conditions are over-specified, i.e., discrete solutions at boundary control volumes and, possibly, at their neighbors are specified from the manufactured solution.

IV.A. Discretization error

The main accuracy measure is the *discretization error*, E_d, which is defined as the difference between the exact discrete solution, U^h, of the discretized equations (3) and the exact continuous solution, U, to the corresponding differential equations,

$$E_d = U - U^h, \tag{7}$$

where U is sampled at mesh nodes.

IV.B. Truncation error

Another accuracy measure commonly used in computations is *truncation error*. Truncation error, E_t, characterizes the accuracy of approximating the differential equation (2). For finite differences, it is defined as the residual obtained

after substituting the exact solution U into the discretized differential equations.[30] For FVD schemes, the traditional truncation error is usually defined from the time-dependent standpoint.[31,32] In the steady-state limit, it is defined (e.g., in [33]) as the residual computed after substituting U into the normalized discrete equations (3),

$$E_t = \frac{1}{V}\left[-\int_{\Omega} f^h \, d\Omega + \oint_{\partial\Omega} \left(\mathbf{F^h}\cdot\hat{\mathbf{n}}\right)\, ds\right], \tag{8}$$

where V is the measure of the control volume,

$$V = \int_{\Omega} d\Omega, \tag{9}$$

f^h is an approximation of the forcing function f on Ω, and the integrals are computed according to some quadrature formulas. Truncation and discretization errors are related through the error transport equation[34]

$$L_h\left(E_d\right) = -E_t, \tag{10}$$

where L_h is the linearization of the discrete governing equations.

It has been long known that convergence of truncation errors severely degrades on irregular (low-quality) meshes. Such degradation, however, does not necessarily imply a less than design order convergence of discretization errors. Plentiful computational evidence and a solid body of theory concerning the effect of supra-convergence indicate that, on irregular grids, the design-order discretization-error convergence can be achieved even when truncation errors exhibit a lower-order convergence or, in some cases, do not converge at all.[9–11]

IV.C. Accuracy of gradient reconstruction

The accuracy of the gradient approximation is also important. The accuracy for an ULSQ gradient is evaluated by comparing the reconstructed gradient, $\nabla^{\mathbf{r}}U$, with the exact gradient, ∇U, computed at the node. The accuracy of a GG gradient is evaluated at an element. The reconstructed and exact gradients are compared at the element center computed as the average of the element vertexes. In accuracy evaluation, the gradient reconstruction uses a sampling of the exact solution U at the nodes on a given grid. The error in the gradient reconstruction is measured as

$$E_{\mathrm{g}} = \|\epsilon_g\|, \tag{11}$$

where function ϵ_g is the amplitude of the gradient error evaluated at a node,

$$\epsilon_g = |\nabla^{\mathbf{r}}U - \nabla U|, \tag{12}$$

and $\|\cdot\|$ is a norm of interest.

V. Class A: Isotropic Grids in Rectangular Geometry

V.A. Grid and solution specifications

Sequences of consistently refined[19] grids with $5^2, 9^2, 17^2, 33^2, 65^2, 129^2$, and 257^2 nodes are generated on the unit square $[0,1]\times[0,1]$. Irregularities are introduced at each grid independently, so the grid metrics remain discontinuous on all irregular grids. With the random perturbation range limited by a quarter of the local mesh size, the angles of triangular elements can approach 180° and the ratio of the neighboring cell volumes can be arbitrarily high.

The exact solutions is $U = \sin(\pi x - 2\pi y)$, so for the inviscid Eq. 1 with $\mathbf{a} = (2,1)$, the force is $f = 0$, and for the viscous Eq. 2, $f = -5\pi^2\sin(\pi x - 2\pi y)$. The numerical tests evaluating truncation and discretization errors are performed with boundary conditions over-specified from the manufactured solution for all nodes linked to the boundary.

V.B. Gradient reconstruction accuracy

Figure 2 shows the variation of the L_1 norm of the gradient error. As expected, the ULSQ gradient reconstruction with a quadratic fit is second-order accurate on all grids. The GG gradient reconstruction is second order only on perfect grids of type (I); on all other grids, the GG gradients are first-order accurate. All equivalent-order methods provide very similar errors. Thus, no mesh quality effects are observed for the L_1 norm of the gradient error on isotropic grids. Although not shown, the observed L_∞ norms of the gradient errors converge with the same orders as the corresponding L_1 norms, but the L_∞ norms of GG gradient error on grids of types (III_p) and (IV_p) are an order of magnitude greater than the L_∞ norms of other first-order errors. The latter effect is caused by gradient accuracy deterioration on triangular elements with obtuse angles approaching $180°$. Theoretically, with an infinitesimal probability, the GG gradient error may become infinitely large at an element with a vanishing volume.

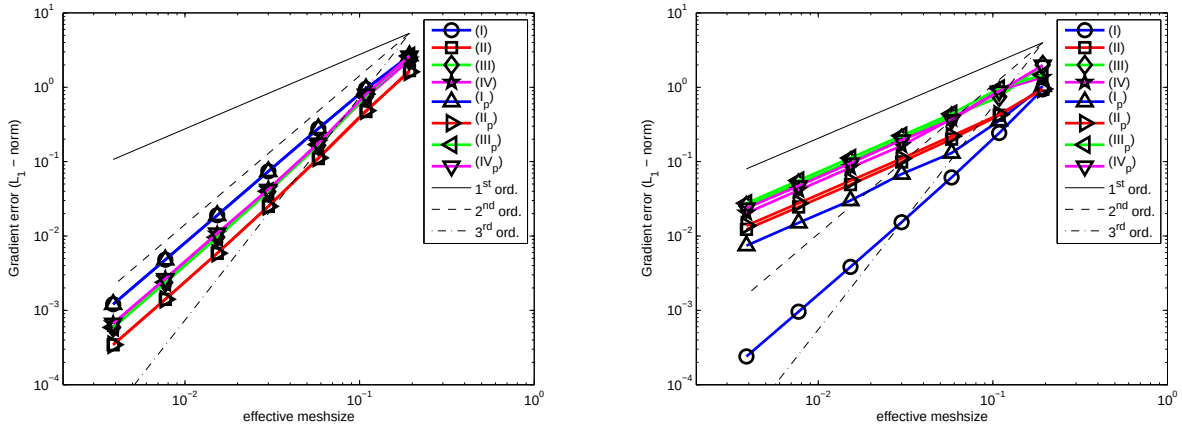

(a) ULSQ-quadratic fit at node

(b) GG at element

Figure 2. Accuracy of gradient reconstruction on isotropic grids. Manufactured solution is $U = \sin(\pi x - 2\pi y)$.

V.C. Truncation errors

The truncation errors are extremely sensitive to mesh quality. Convergence rates of the L_1 norm of truncation errors for inviscid and viscous fluxes are shown in Figures 3 and 4, respectively. The inviscid errors converge with the third order only on regular triangular meshes of type (II). On irregular triangular grids of types (III), (II_p), and (III_p) and on perfect quadrilateral grid of type (I), the inviscid truncation errors converge with the second order. Irregularities on grids with quadrilateral elements (types (IV), (I_p), and (IV_p)) lead to the zeroth-order convergence.

Similar sensitivity is observed for the truncation errors of viscous fluxes discretized by the Avg-LSQ scheme with the second-order accurate ULSQ gradients (Figures 4(a) and 4(b)). The second-order convergence is observed only on perfectly regular grids of types (I) and (II). The convergence deteriorates to the first order on irregular triangular grids and to the zeroth order on mixed-element and perturbed quadrilateral grids. For the viscous fluxes discretized with the GG scheme (Figures 4(c) and 4(d)), truncation errors do not converge on any but perfectly regular grids of types (I) and (II). Note that GG scheme produces identical discretizations on grids of types (I), (II), and (III).[15] Thus, corresponding GG solutions and truncation errors on grids of types (I) and (II) are always identical. Different results on grids of type (III) are explained by the differences in the dual volumes.

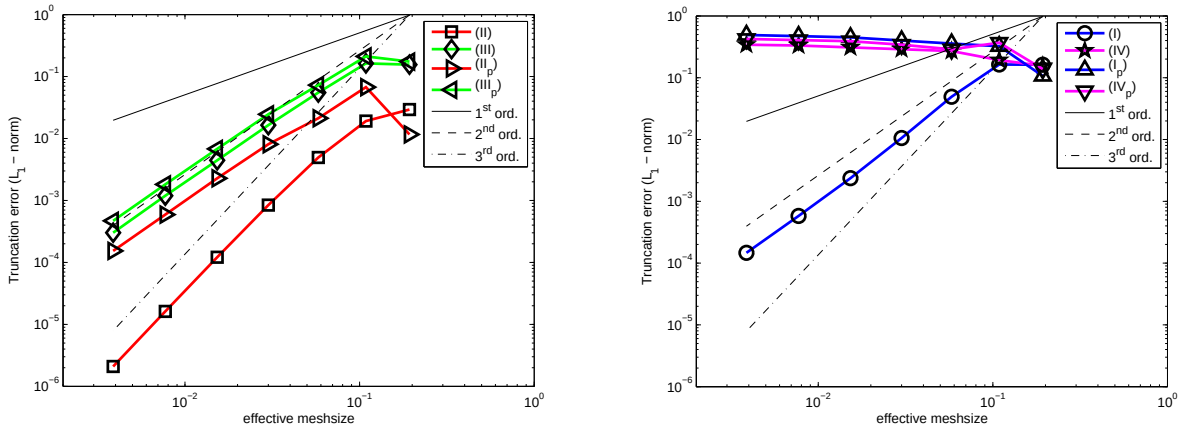

(a) Triangular grids

(b) Mixed and quadrilateral grids

Figure 3. Inviscid truncation errors on isotropic grids. Manufactured solution is $U = \sin(\pi x - 2\pi y)$.

V.D. Discretization errors

Convergence rates of the L_1 norm of discretization errors for inviscid and viscous fluxes are shown in Figures 5 and 6, respectively. Discretization errors for viscous fluxes show no sensitivity to mesh quality. The errors for both Avg-LSQ and GG schemes are practically identical to the plotting accuracy for all grids. The accuracy of inviscid solutions deteriorates on meshes with quadrilateral elements. This is not a surprise because the inviscid scheme used in this study is designed to be third order only on simplicial grids.[21,22] The edge-based integration scheme used in this scheme is known to deteriorate to first order on grids of types (I_p), (IV), and (IV_p).[18,19,27] On triangular grids, the discretization accuracy of inviscid solutions is not sensitive to mesh quality. If anything, discretization errors are somewhat smaller on topologically structured grids of types (II) and (II_p).

VI. Class B: Anisotropic Grids in Rectangular Geometry

This section considers FVD schemes on irregular stretched grids generated on rectangular domains. Figure 7 shows an example grid with the maximal aspect ratio $\mathcal{A} = 1000$. A sequence of consistently refined stretched grids is generated on the rectangle $(x, y) \in [0, 1] \times [0, 0.5]$ in the following 3 steps.

1. A background regular rectangular grid with $N = (N_x + 1) \times (N_y + 1)$ nodes and the horizontal mesh spacing $h_x = \frac{1}{N_x}$ is stretched toward the horizontal line $y = 0.25$. The y-coordinates of the horizontal grid lines in the top half of the domain are defined as

$$y_{\frac{N_y}{2}+1} = 0.25; \qquad y_j = y_{j-1} + \hat{h_y}\beta^{j-\left(\frac{N_y}{2}+1\right)}, \qquad j = \frac{N_y}{2} + 2, \ldots, N_y, N_y + 1. \tag{13}$$

   Here $\hat{h_y} = \frac{h_x}{A}$ is the minimal mesh spacing between the vertical lines, $\mathcal{A} = 1000$ is a fixed maximal aspect ratio, and β is a stretching factor which is found from the condition $y_{N_y+1} = 0.5$. The stretching in the bottom half of the domain is defined analogously.

2. Irregularities are introduced by random shifts of interior nodes in the vertical and horizontal directions. The vertical shift is defined as $\Delta y_j = \frac{3}{16}\rho \min(h_y^{j-1}, h_y^j)$, where ρ is a random number between -1 and 1, and h_y^{j-1}

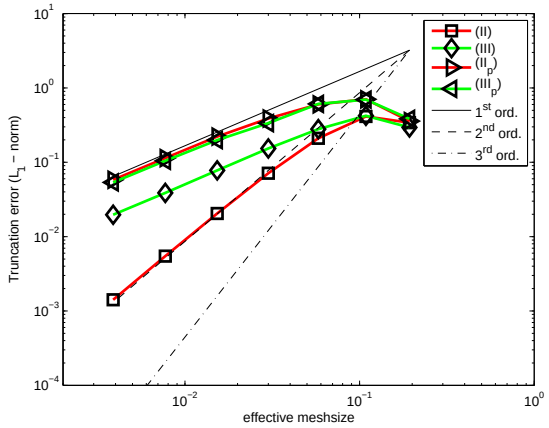

(a) Avg-LSQ; triangular grids

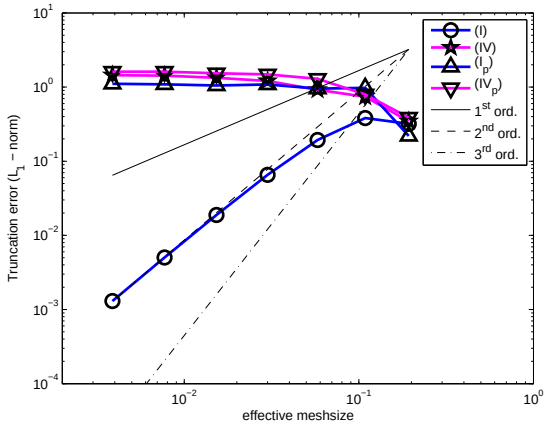

(b) Avg-LSQ; mixed and quadrilateral grids

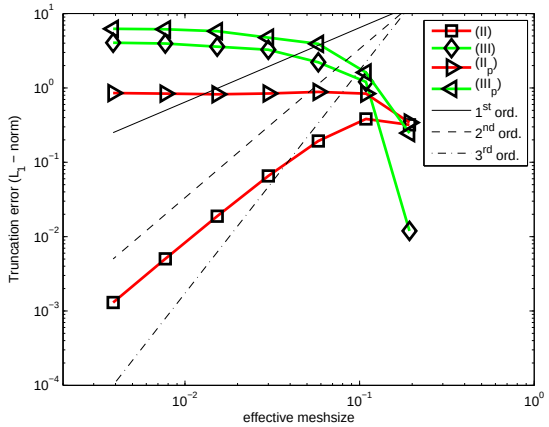

(c) GG; triangular grids

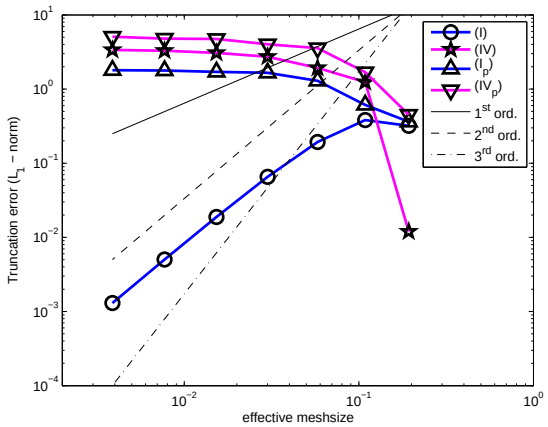

(d) GG; mixed and quadrilateral grids

Figure 4. Viscous truncation errors on isotropic grids. Manufactured solution is $U = \sin(\pi x - 2\pi y)$.

and h_y^j are vertical mesh spacings on the background stretched mesh around the grid node. The horizontal shift is introduced analogously, $\Delta x_i = \frac{3}{16}\rho h_x$. With these random node perturbations, all perturbed quadrilateral cells are convex.

3. Each perturbed quadrilateral is randomly triangulated with one of the two diagonal choices; each choice occurs with a probability of one half.

Sequences of consistently refined stretched grids with maximum aspect ratio $\mathcal{A} = 1000$ including $9 \times 65, 17 \times 129, 33 \times 257$, 65×513, and 129×1025 nodes have been considered. The corresponding stretching ratios are $\beta \approx 1.207, 1.098, 1.048, 1.025$, and 1.012. The aspect ratio near the external horizontal boundaries is about 2.7.

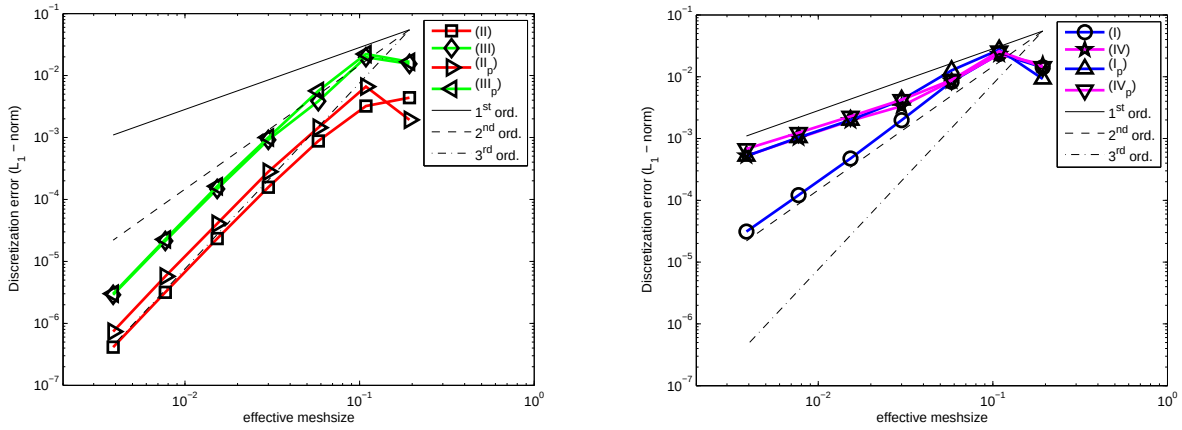

(a) Triangular meshes

(b) Mixed and quadrilateral meshes

Figure 5. Inviscid discretization errors on isotropic grids. Manufactured solution is $U = \sin(\pi x - 2\pi y)$.

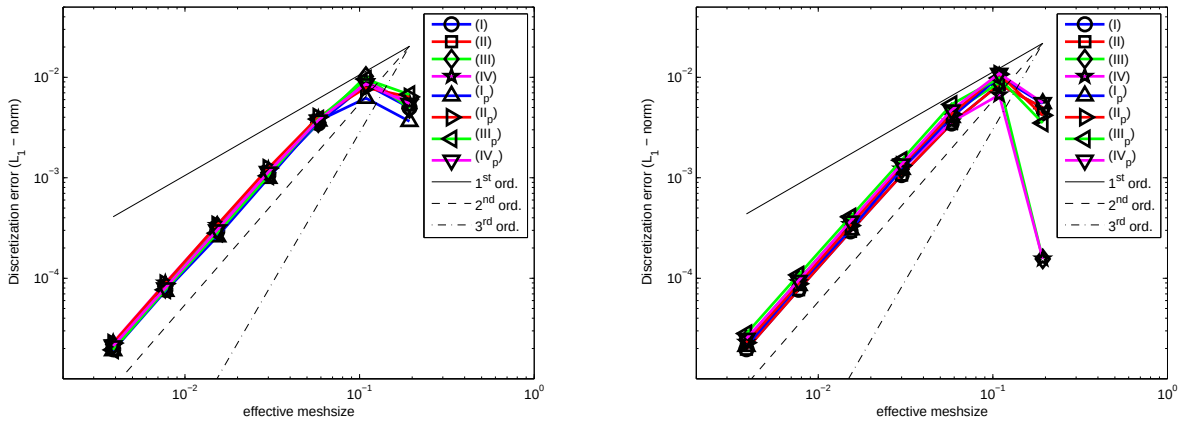

(a) Avg-LSQ

(b) GG

Figure 6. Viscous discretization errors on isotropic grids. Manufactured solution is $U = \sin(\pi x - 2\pi y)$.

In the tests on grids of Class (B) performed with either the manufactured solution $\sin(\pi x - 2\pi y)$ or extended over-specification used in tests on grid of Class (A), the asymptotic behavior of the discretizations errors for viscous fluxes was not observed on coarse grids. The exhibited discretization errors were uncharacteristically low on coarse grids, but did not converge with the asymptotic order. The manufactured solution has been changed to $U = \cos(\pi x - 2\pi y)$. Also only solutions at boundary nodes are over-specified. With these changes, the asymptotic behavior of the discretizations errors for the GG viscous fluxes is established on relatively coarse grids. Note that the force term for inviscid equations is still $f = 0$ for $\mathbf{a} = (2, 1)$.

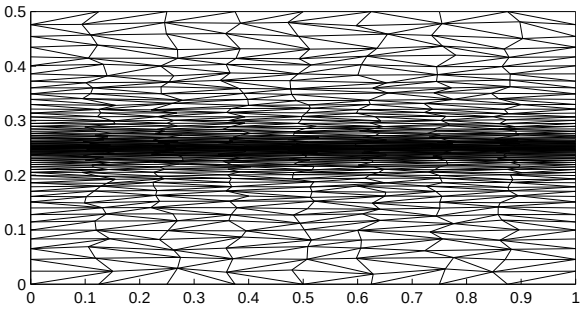

Figure 7. Stretched grid of type (III_p) with 9×65 nodes.

The convergence plots of truncation errors are not shown for tests of Class (B). The qualitative behavior (orders of convergence) of truncation errors is the same as on isotropic grids, shown in Figures 3 and 4 The magnitude of the errors is increased by three orders of magnitude, proportional to the aspect ratio $\mathcal{A} = 1000$.

VI.A. Gradient reconstruction accuracy

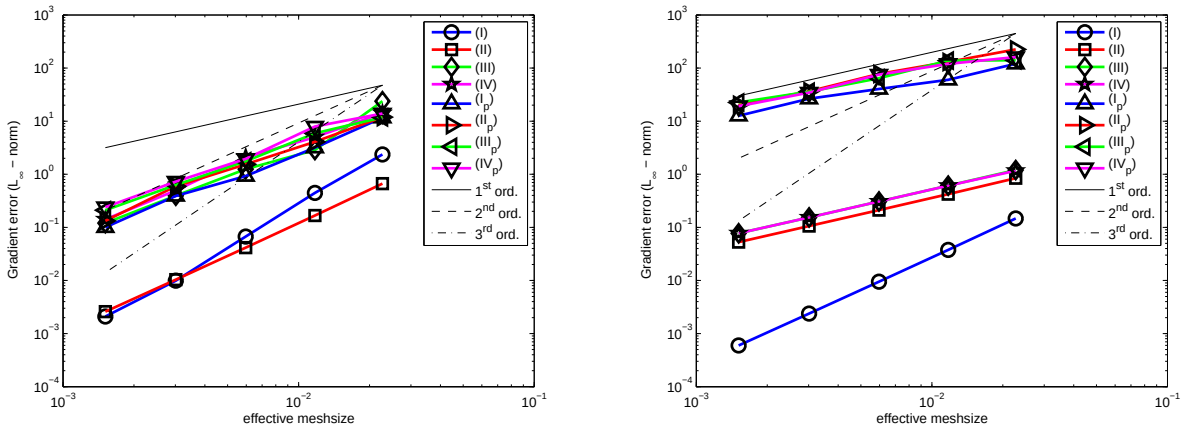

(a) ULSQ-quadratic fit at node

(b) GG at element

Figure 8. Accuracy of gradient reconstruction on stretched grids with maximum aspect ratio $A = 1000$. Manufactured solution is $U = \cos(\pi x - 2\pi y)$.

A recent study[20] assessed the accuracy of gradient approximations on various irregular grids with high aspect ratio $\mathcal{A} = \frac{h_x}{h_y} \gg 1$. The study indicates that for rectangular geometries and functions predominantly varying in

the direction of small mesh spacing (y-direction here), gradient reconstruction is accurate, providing small relative error converging with at least first order in consistent refinement on grids of all types. For manufactured solutions significantly varying in the direction of larger mesh spacing (x-direction), the gradient reconstruction may produce extremely large $O(\mathcal{A}h_x^p)$ relative errors affecting the accuracy of the y-directional gradient component. Here, p is the formal gradient reconstruction order; $p = 1$ for the GG scheme and $p = 2$ for the ULSQ scheme with a quadratic fit.

A summary of the results concerned with gradient accuracy on anisotropic grids is presented in Table 1. For reference, the data concerning the ULSQ method with a linear fit are also shown. The gradient is accurately reconstructed on all unperturbed grids by the the GG scheme at element. All considered gradient reconstruction methods may generate large relative errors on perturbed grids of types $(I_p) - (IV_p)$.

Table 1. Relative error of gradient reconstruction on anisotropic grids for solutions with significant variation in the x-direction of larger mesh spacing.

Grid Types	(I)	(II)	(III)	(IV)	$(I_p) - (IV_p)$
ULSQ-linear fit at node	$O(h_x^2)$	$O(h_x^2)$	$O(\mathcal{A}h_x)$	$O(\mathcal{A}h_x)$	$O(\mathcal{A}h_x)$
ULSQ-quadratic fit at node	$O(h_x^2)$	$O(h_x^2)$	$O(\mathcal{A}h_x^2)$	$O(\mathcal{A}h_x^2)$	$O(\mathcal{A}h_x^2)$
GG at element	$O(h_x^2)$	$O(h_x)$	$O(h_x)$	$O(h_x)$	$O(\mathcal{A}h_x)$

The convergence of L_∞ norm of gradient errors is shown in Figure 8. The L_∞ norm is used to highlight the worst gradients observed in high-aspect ratio regions of the stretched grids of Class (B). All ULSQ gradients converge with second order, but the magnitude of the gradient errors is sensitive to grid quality. As shown in Table 1, with any deviation from the regularity of grids of types (I) and (II), the ULSQ gradient error becomes proportional to aspect ratio. The GG gradients converge with the first order on all grids beside the grids of type (I), where the second-order convergence is observed. In spite of the lower order convergence, the GG gradients show a clear advantage over the ULSQ gradients on coarse unperturbed grids of types $(I) - (IV)$. The GG scheme on such grids provides gradient accuracy independent of aspect ratio. On perturbed grids of types $(I_p) - (IV_p)$, the GG errors are also proportional to the aspect ratio, and ULSQ gradients are preferable.

VI.B. Discretization errors

The convergence of the L_1 norm of discretizations errors for inviscid fluxes is shown in Figure 9. The convergence characteristics are similar to those exhibited on isotropic grids of Class (A). Third-order convergence insensitive to grid irregularities is observed on all triangular grids of types $(II), (III), (II_p)$, and (II_p). Convergence on grids of type (I) is second order, but any irregularity on mixed and quadrilateral meshes degrades the convergence to the first order.

The convergence of the L_1 norm of discretization errors for viscous fluxes is shown in Figure 10. All discretization errors converge with the second order. While second-order convergence of the Avg-LSQ scheme is not apparent in Figure 10(a) on triangular and mixed-element grids, the second-order slope has been attained on finer grids. For reference, convergence of the errors obtained with a linear fit on grids of type (II) is also shown. The Avg-LSQ errors are relatively small only on pure quadrilateral grids of types (I) and (I_p). The magnitude of errors obtained with a quadratic fit is much smaller than the magnitude of errors obtained with a linear fit. However, discretization errors of the GG scheme are significantly better than any the Avg-LSQ errors. The GG errors are clearly divided into two groups. The errors on unperturbed grids of types $(I) - (IV)$ are small on all grids; the errors on perturbed grids are roughly two orders of magnitude higher for any given number of degrees of freedom. The ratio is about the same as the ratio between gradient errors shown in Figure 8(b).

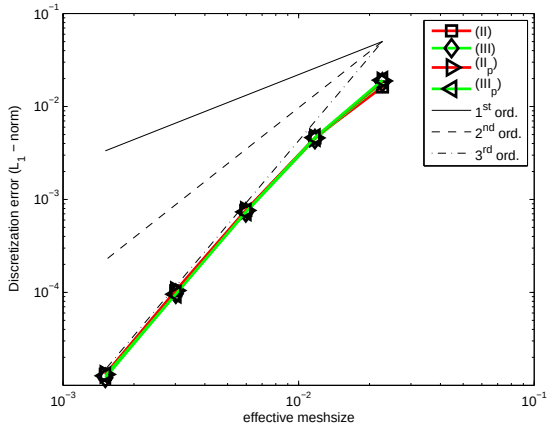

(a) Triangular meshes

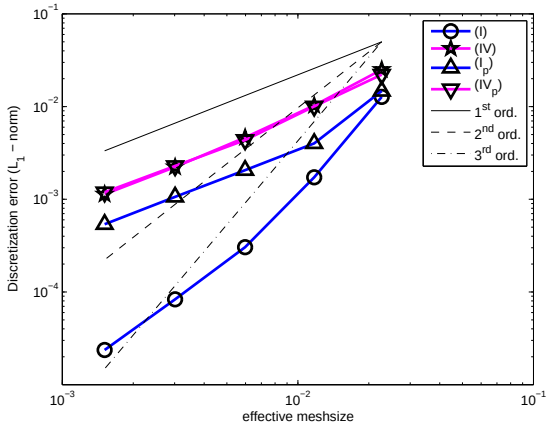

(b) Mixed and quadrilateral meshes

Figure 9. Inviscid discretization errors on anisotropic stretched grids with maximum aspect ratio $\mathcal{A} = 1000$. Manufactured solution is $U = \cos(\pi x - 2\pi y)$.

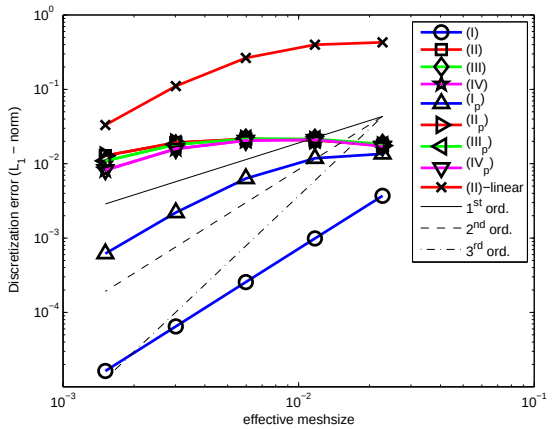

(a) Avg-LSQ

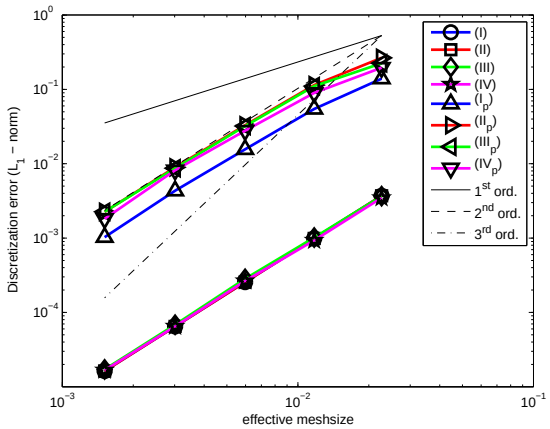

(b) GG

Figure 10. Viscous discretization errors on anisotropic stretched grids with maximum aspect ratio $\mathcal{A} = 1000$. Manufactured solution is $U = \cos(\pi x - 2\pi y)$.

VII. Class C: Grids with Curvature and High Aspect Ratio

VII.A. Grid and solution specification

In this section, we discuss FVD schemes on grids with curvature and high aspect ratio. The grid nodes are generated from a cylindrical mapping, where (r, θ) denote polar coordinates with spacings of h_r and h_θ, respectively. The grid aspect ratio is defined as the ratio of mesh sizes in the circumferential and the radial directions, $\mathcal{A} = Rh_\theta/h_r$, where R is the radius of curvature.

A measure of the curvature-induced mesh deformation is Γ defined as:

$$\Gamma = \frac{R\,(1-\cos(h_\theta))}{h_r} \approx \frac{R h_\theta^2}{2h_r} = \mathcal{A}\frac{h_\theta}{2}. \tag{14}$$

The following assumptions are made about the range of parameters: $R \approx 1$, $\mathcal{A} \gg 1$, and $\Gamma h_r \ll 1$, which implies that both h_r and h_θ are small. For a given value of $\mathcal{A}$, the parameter Γ may vary: $\Gamma \ll 1$ indicates meshes that are locally (almost) non-deformed. As a practical matter, grids with $\Gamma < 0.2$ can be considered as nominally non-curved. In a mesh refinement that keeps $\mathcal{A}$ fixed, $\Gamma = O(\mathcal{A}h_\theta)$ asymptotes to zero. This property implies that on fine enough grids with fixed curvature and aspect ratio, the error convergence is expected to be the same as on similar grids generated on rectangular domains with no curvature.

Four basic types of 2-D grids are studied in the cylindrical geometry. Unlike the computational grids used in the rectangular geometry, random node perturbation is not applied to high-Γ grids because even small perturbations in the circumferential direction may lead to non-physical control volumes.

The manufactured solution considered in this section is $U = \sin(5\pi r)$. The convection direction is changed to a variable tangential direction $\mathbf{a} = (\frac{y}{r^2}, -\frac{x}{r^2})$, so the inviscid force term remains zero. Solutions at boundary nodes are over-specified.

VII.B. Gradient reconstruction accuracy

Table 2. Relative errors of gradient reconstruction for manufactured solutions varying only in the radial direction on grids corresponding to $1 \le \Gamma \le 50$.

Grid Types	(I)	(II)	(III)	(IV)
ULSQ-linear fit	$O(1)$	$O(1)$	$O(1)$	$O(1)$
ULSQ-quadratic fit	$O(h_\theta)$	$O(h_\theta)$	$O(h_\theta)$	$O(h_\theta)$
GG	$O(h_\theta^2)$	$O(h_\theta)$	$O(h_\theta)$	$O(h_\theta)$

Our main interest is solutions varying predominantly in the radial direction on grids with $\Gamma \gg 1$ corresponding to meshes with large curvature-induced deformation. Computations and analysis reported earlier[17,35,36] concluded that the ULSQ gradient approximation with a linear fit is zeroth-order accurate for such solutions. The use of the ULSQ method with a quadratic fit dramatically improves gradient accuracy on high-Γ grids leading to a first-order convergence of gradient errors on grids with $1 \le \Gamma \le 50$. The errors of gradient reconstruction for a radial solution are summarized in Table 2. The ULSQ gradient errors do not show order properties on high-Γ grids. This is in contrast to the convergence on low-Γ grids shown in Table 1. The magnitudes of the relative errors for the GG scheme and for the ULSQ scheme with a quadratic fit are much smaller than the magnitude for the ULSQ scheme with a linear fit.

The computational tests are performed with the methodology of downscaling.[19,20] on a sequence of narrow arc-shaped domains with the angular extent of $\frac{\pi}{9}L$ radians and the radial extent of $1 \le r \le 1 + \frac{\pi}{9}L\mathcal{A}^{-1}$. The scale L changes as $L = 2^{-n}, n = 0, \ldots, 8$. On each domain, a 17×17 grid is generated with nodes uniform spaced in the polar coordinates. Figure 11 shows convergence of the L_∞ norms of gradient errors computed for the manufactured solution $U = \sin(5\pi r)$ on grids with aspect ratios $\mathcal{A} = 100$ and $\mathcal{A} = 1000$. The errors are shown versus the grid deformation parameter, Γ, defined in Eq. 14. Figures 11(a) and 11(b) show convergence of ULSQ gradient errors computed with quadratic and linear fits on grids of types $(I) - (IV)$. Figures 11(c) and 11(d) show convergence of GG gradient errors. As known from previous studies,[15–17,35,36] the errors of GG gradients are small and show the order property on all grids. The ULSQ gradients computed with a linear fit lose accuracy on high-Γ grids. The ULSQ gradients computed with a quadratic fit do not recover the order property on high-Γ grids, but show the smallest error magnitudes on grids of types $(II), (III)$, and (IV). The GG gradients show the smallest errors on regular quadrilateral grids of type (I).

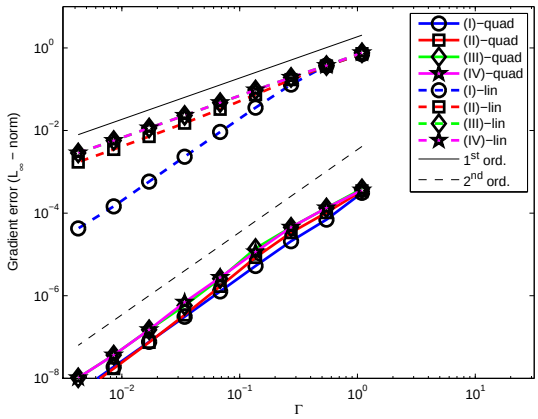

(a) ULSQ at node, $\mathcal{A} = 100$

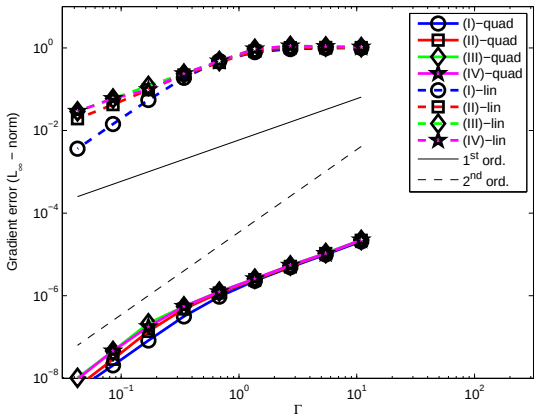

(b) ULSQ at node, $\mathcal{A} = 1000$

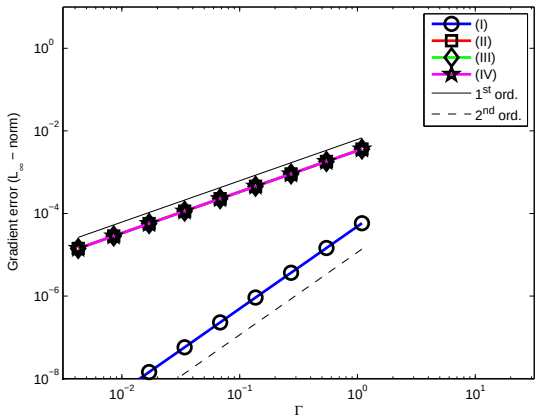

(c) GG at element, $\mathcal{A} = 100$

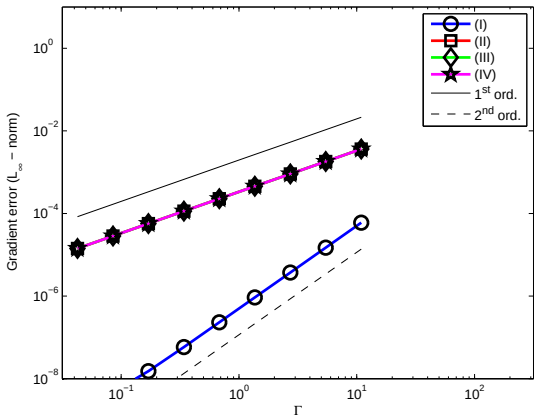

(d) GG at element, $\mathcal{A} = 1000$

Figure 11. Accuracy of gradient reconstruction on high-Γ grids. Manufactured solution is $U = \sin(5\pi r)$.

VII.C. Discretization Errors

Computational grids used in the grid-refinement study of discretization errors are radially stretched grids with a radial extent of $1 \leq r \leq 1.2$ and an angular extent of $20°$. Fixed maximal aspect ratios are used. The maximal aspect ratio is $\mathcal{A} \approx 1000$ for viscous computations. The grids have four times more cells in the radial direction than in the circumferential direction. The maximum value of Γ changes approximately as $\Gamma \approx 22, 11, 5.5, \ldots$. The corresponding grid stretching ratios change as $\beta = 1.25, 1.11, 1.06, \ldots$. Representative grids of types (III) and (IV) are shown in Figure 12.

The third-order inviscid scheme produces highly accurate solutions, so local errors become very small on relatively coarse highly stretched grids and convergence is obscured by round-off errors interfering with the solutions. A reduced

(a) Grid of type (III).

(b) Grid of type (IV).

Figure 12. Representative 9×33 irregular stretched high-Γ grids.

maximal aspect ratio of $\mathcal{A} \approx 100$ has been chosen for inviscid computations.

Convergence of the L_1 norm of discretization errors is shown in Figures 13 and 14 for inviscid and viscous fluxes, respectively. Excellent second-order convergence is observed for both viscous schemes on all grids. The inviscid errors converge with (almost) fourth order on grids of type (I), with third order on grids of types (II) and (III), and with first order on grids of type (IV). The unusually high order of convergence on grids of type (I) is explained by the fact that, for a manufactured solution varying in the radial direction only, the inviscid scheme on grids of type (I) turns into a fourth-order pure one-dimensional scheme. Any solution variation in the circumferential direction brings the expected second-order convergence on grids of type (I). Note that, because of asymmetric gradient-reconstruction stencil, the scheme does not become one-dimensional on grids of types (II) and (III), and, thus, its (third) order of convergence on these grids is independent of solution variation.

VIII. Conclusions

The effects of mesh irregularities on accuracy of unstructured node-centered finite-volume discretizations have been considered for edge-based schemes that use unweighted least-squares gradient reconstruction with a quadratic fit. The inviscid scheme is nominally third-order accurate on general triangular meshes.[21,22] The viscous scheme is a nominally second-order accurate discretization that uses an average-least-squares method with a face-tangent augmentation[24,25] for viscous fluxes. The results have been contrasted with a common Green-Gauss discretization scheme and previous studies for the unweighted least-squares gradient reconstruction with a linear fit. Gradient errors, truncation errors, and discretization errors have been separately studied according to a previously introduced methodology.[15,16]

The methodology considers three classes of grids: Class (A) includes isotropic grids in a rectangular geometry. Class (B) includes anisotropic grids representative of adaptive-grid simulations. Class (C) includes anisotropic advancing-layer grids representative of high-Reynolds number turbulent flow simulations over a curved body. Regular and irregular grids have been considered, including mixed-element grids and grids with random perturbations of nodes. Grid perturbations and stretching have been introduced independently of solution variation to bring out the worst possible behavior.

Gradient errors are largely insensitive to mesh irregularities on isotropic grids of Class (A). The gradient accuracy

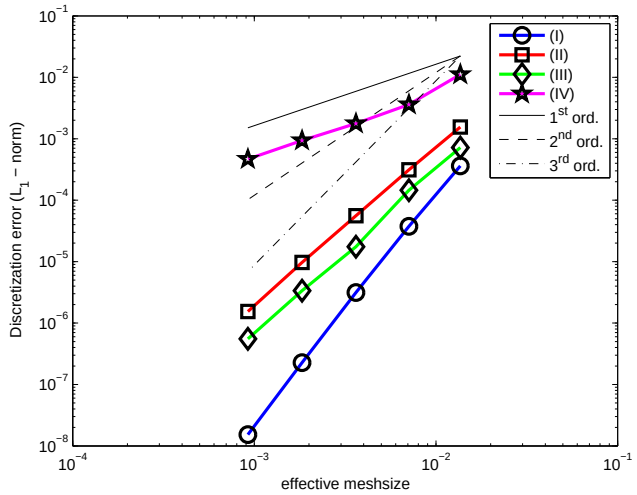

Figure 13. Inviscid discretization errors on high-Γ stretched grids with maximum aspect ratio $\mathcal{A} = 100$. Manufactured solution is $U = \sin(5\pi r)$.

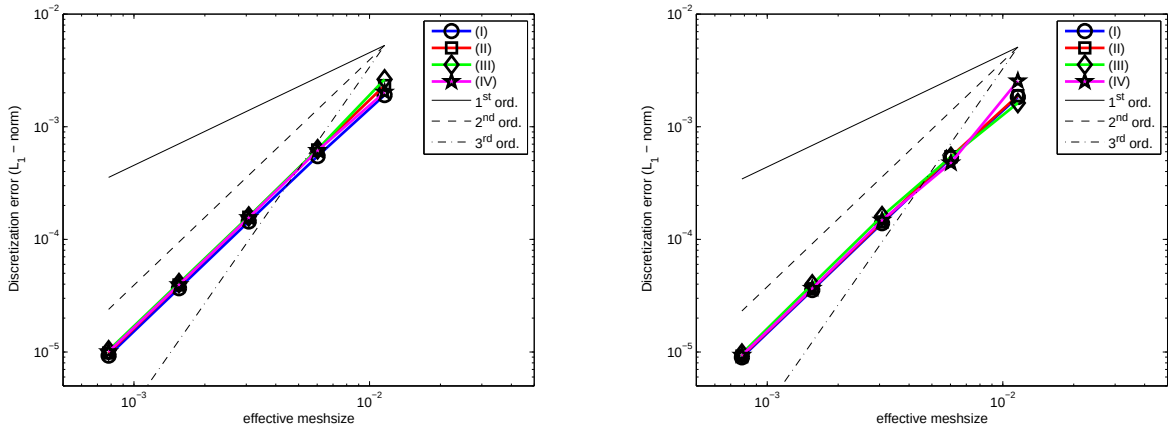

(a) Avg-LSQ

(b) GG

Figure 14. Viscous discretization errors on high-Γ stretched grids with maximum aspect ratio $\mathcal{A} = 1000$. Manufactured solution is $U = \sin(5\pi r)$.

deteriorates with high aspect ratio in combination with node perturbation. On grids of class (B), the gradient errors converge with at least first order for the Green-Gauss and the least-squares scheme with a linear fit and with second order for the least-squares scheme with a quadratic fit. The least-squares gradient errors become proportional to the aspect ratio on all irregular grids. On grids with node perturbation, all gradient errors are proportional to the aspect ratio. On class (C) grids characterized by a high deformation parameter Γ, the Green-Gauss gradient errors converge with at least first order and are small on all grids. The least-squares gradient errors for radial solutions show no order properties; the magnitude of the errors with a quadratic fit is inversely proportional to the square of the aspect ratio, which is superior to the $O(1)$ magnitude observed with a linear fit. Although not considered here, the approximate-

mapping approach to gradient reconstruction[15,16] can recover the second-order convergence of gradient errors on high-Γ grids of Class (C).

As observed previously[8–11,19] and confirmed here, lack of mesh regularity strongly affects truncation errors, which converge with lower-than-design order on all irregular meshes. Viscous truncation errors do not converge at all on perturbed grids.

Inviscid discretization errors are practically insensitive to mesh irregularity on triangular grids, demonstrating the third-order convergence and small variation of the error magnitudes. Discretization accuracy is more sensitive to mesh irregularity on grids with quadrilateral elements. On those grids, the results observed with the least-squares method with a quadratic fit show no advantage over previous results obtained with a linear fit,[16,19] both showing first-order convergence on mixed and perturbed quadrilateral grids.

In all cases, the viscous discretization errors asymptotically converge with second order. Similar to the gradient accuracy, the magnitude of discretization errors of viscous solutions is insensitive to grid irregularities on grids of class (A), but may be sensitive on grids of classes (B) and (C). On such grids, the Green-Gauss method is the most accurate, although, the errors on the grids with node perturbation are still significantly larger than errors on grids with unperturbed nodes. Asymptotically, the difference is proportional to the aspect ratio. Accuracy of the average-least-squares methods deteriorates on irregular high-aspect-ratio grids, although the deterioration is less with a quadratic fit than with a linear fit.

The following recommendations are offered: (1) The unweighted least-squares method with a quadratic fit is highly recommended as a robust way to compute accurate gradients on all grids. (2) The edge-based scheme based on the unweighted least-squares method with a quadratic fit is recommended for inviscid fluxes. It produces accurate solutions and is insensitive to deterioration of mesh quality on triangular grids. (3) The Green-Gauss scheme is recommended for viscous fluxes. On isotropic and advanced-layer grids of classes (A) and (C), both Green-Gauss and averaged-least-squares methods produce uniformly second-order solutions and are insensitive to mesh irregularities. On grids of class (B), there is a sensitivity to grid irregularities; the Green-Gauss solutions are less sensitive than averaged-least-squares solutions.

The overall conclusion is that relations between mesh characteristics and solution accuracy are complicated. The mesh irregularities affect gradient, truncation, and discretization errors in dramatically different ways. The resolution is expected in the form of adjoint-based grid adaptation that directly and rigorously connects the local mesh properties with the desired solution outcome.

References

[1] Fidkowski, K. J. and Darmofal, D. L., "Review of Output-Based Error Estimation and Grid Adaptation in Computational Fluid Dynamics," *AIAA Journal*, Vol. 49, No. 4, 2011, pp. 673–694.

[2] Park, M., Lee-Rausch, E. M., and Rumsey, C. L., "FUN3D and CFL3D Computations for the First High Lift Prediction Workshop," AIAA Paper 2011-936, 49-th AIAA Aerospace Science Meeting and Exhibit, Orlando, FL, January 2011.

[3] Berzins, M., "Mesh Quality: A function of Geometry, Error Estimates, or Both?" *Engineering with Computers*, Vol. 15, No. 3, 1999, pp. 236–247.

[4] Knupp, P. M., "Algebraic Mesh Quality Measures," *SIAM J. Sci. Comp.*, Vol. 23, No. 1, 2001, pp. 193–218.

[5] Knupp, P. M., "Remarks on Mesh Quality," 45-th AIAA Aerospace Science Meeting and Exhibit, Reno, NV, January 2007.

[6] Mastin, C. W., "Error induced by coordinate system," *Numerical Grid Generation*, edited by J. Thompson, North-Holand, New York, 1982, pp. 31–40.

[7] Lee, J. and Tsuei, Y., "A Formula for Estimation of Truncation Errors of Convection Terms in a Curvilinear Coordinate System," *J. Comput. Phys.*, Vol. 98, 1992, pp. 90–100.

[8] Diskin, B. and Thomas, J. L., "Notes on Accuracy of Finite Volume Discretization Schemes on Irregular Grids," *Appl. Num. Math.*, Vol. 60, No. 3, 2009, pp. 224–226.

[9] Forsyth, P. A. and Sammon, P. H., "Quadratic convergence for cell-centered grids," *Appl. Num. Math.*, Vol. 4, 1988, pp. 377–394.

[10] Kreiss, H. O., Manteuffel, T. A., Wendroff, B., and White, A. B., "Supra-convergence schemes on irregular grids," *Mathematics of Computations*, Vol. 47(176), October 1986, pp. 537–554.

[11] Manteuffel, T. A. and White, A. B., "The numerical solution of the second-order boundary value problem on nonuniform meshes," *Mathematics of Computations*, Vol. 47(176), October 1986, pp. 511–536.

[12]Babushka, I. and Aziz, A. K., "On the angle condition in the finite element method," *SIAM J. Numer. Anal.*, Vol. 13, April 1976, pp. 214–226.

[13]Krizek, M., "On the maximum angle condition for linear tetrahedral elements," *SIAM J. Numer. Anal.*, Vol. 29, No. 2, April 1992, pp. 513–520.

[14]Berzins, M., "Solution-Based Mesh Quality Indicators for Triangular and Tetrahedral Meshes," *International Journal of Computational Geometry and Applications*, Vol. 10, No. 3, 2000, pp. 333–346.

[15]Diskin, B., Thomas, J. L., Nielsen, E. J., Nishikawa, H., and White, J. A., "Comparison of Node-Centered and Cell-Centered Unstructured Finite-Volume Discretizations: Viscous Fluxes," *AIAA Journal*, Vol. 48, No. 7, 2010, pp. 1326–1338.

[16]Diskin, B. and Thomas, J. L., "Comparison of Node-Centered and Cell-Centered Unstructured Finite-Volume Discretizations: Inviscid Fluxes," *AIAA Journal*, Vol. 49, No. 4, 2011, pp. 836–854.

[17]Mavriplis, D. J., "Revisiting the Least-Square Procedure for Gradient Reconstruction on Unstructured Meshes," AIAA Paper 2003-3986.

[18]Diskin, B. and Thomas, J. L., "Accuracy Analysis for Mixed-Element Finite-Volume Discretization Schemes," NIA Report 2007-08, National Institute of Aerospace, August 2007.

[19]Thomas, J. L., Diskin, B., and Rumsey, C. L., "Towards Verification of Unstructured-Grid Solvers," AIAA Paper 2008-0666.

[20]Diskin, B. and Thomas, J. L., "Accuracy of Gradient Reconstruction on Grids with High Aspect Ratio," NIA Report 2008-12, National Institute of Aerospace, December 2008.

[21]Katz, A. and Sankaran, V., "Mesh quality effects on the accuracy of Euler and Navier-Stokes solutions on unstructured meshes," *Journal of Computational Physics*, Vol. 230, No. 20, 2011, pp. 7670–7686.

[22]Katz, A. and Sankaran, V., "An Efficient Correction Method to Obtain a Formally Third-Order Accurate Flow Solver for Node-Centered Unstructured Grids," *Journal on Scientific Computing*, 2011, DOI: 10.1007/s10915-011-9515-1.

[23]Haselbacher, A. C., *A Grid-Transparent Numerical Method for Compressible Viscous Flow on Mixed Unstructured Meshes*, Ph.D. thesis, Loughborough University, 1999.

[24]Nishikawa, H., Diskin, B., and Thomas, J. L., "Critical study of agglomerated multigrid methods for diffusion," *AIAA Journal*, Vol. 48, No. 4, 2010, pp. 839–847.

[25]Thomas, J. L., Diskin, B., and Nishikawa, H., "A Critical Study of Agglomerated Multigrid Methods for Diffusion on Highly-Stretched Grids," *Computers and Fluids*, Vol. 41, 2011, pp. 82–93.

[26]Roe, P. L., "Approximate Riemann solvers, parameter vectors, and difference schemes," *J. Comp. Phys.*, Vol. 43, No. 2, 1981, pp. 357–372.

[27]Aftosmis, M., Gaitonde, D., and Tavares, T. S., "Behavior of linear reconstruction techniques on unstructured meshes," *AIAA Journal*, Vol. 33, 1995, pp. 2038–2049.

[28]Anderson, W. K. and Bonhaus, D. L., "An implicit upwind algorithm for computing turbulent flows on unstructured grids," *Computers and Fluids*, Vol. 23, No. 1, 1994, pp. 1–21.

[29]Trottenberg, U., Oosterlee, C. W., and Schüler, A., *Multigrid*, Academic Press, London, 2000.

[30]Hirsch, C., *Numerical computation of internal and external flows. Vol.1, Fundamentals of numerical discretization*, A Wiley-Interscience publication, John Wiley & Sons, Inc., 605 Third Avenue, New York, NY 10158-0012, USA, 1988.

[31]Syrakos, A. and Goulas, A., "Estimate of the Truncation Error of Finite Volume Discretization of the Navier-Stokes Equations on Collocated Grids," *Int. J. Numer. Meth. Fluids*, Vol. 50, 2006, pp. 103–130.

[32]Turkel, E., "Accuracy of Schemes with Nonuniform Meshes for Compressible Fluid Flows," *Applied Numerical Mathematics*, Vol. 2, 1986, pp. 529–550.

[33]Giles, M. B., "Accuracy of node-based solutions on irregular meshes," *11-th International Conference on Numerical Methods in Fluid Dynamics*, edited by D. L. Dwoyer, M. Y. Hussaini, and R. Voigt, Lecture Notes in Physics, v. 323, Springer-Verlag, 1989, pp. 369–373.

[34]Roy, C., "Review of Discretization Error Estimators in Scientific Computing," 2010, AIAA Paper 2010-0126.

[35]Petrovskaya, N. V., "The choice of weight coefficients for least-square gradient approximation," *J. Math. Mod.*, Vol. 16(5), 2004, pp. 83–93, (in Russian).

[36]Smith, T. M., Barone, M. F., Bond, R. B., Lorber, A. A., and Baur, D. G., "Comparison of Reconstruction Techniques for Unstructured Mesh Vertex Centered Finite Volume Scheme," AIAA Paper 2007-3958.